Molecular Crystals and Liquid Crystals

ISSN: 1542-1406 (Print) 1563-5287 (Online) Journal homepage: http://www.tandfonline.com/loi/gmcl20

Nematic Liquid Crystals under Conical Capillary Confinement: Theoretical Study of Geometry Effects on Disclination Lines

Alireza Shams, Xuxia Yao, Jung Ok Park, Mohan Srinivasarao & Alejandro D. Rey

To cite this article: Alireza Shams, Xuxia Yao, Jung Ok Park, Mohan Srinivasarao & Alejandro D. Rey (2015) Nematic Liquid Crystals under Conical Capillary Confinement: Theoretical Study of Geometry Effects on Disclination Lines, Molecular Crystals and Liquid Crystals, 612:1, 56-63, DOI: 10.1080/15421406.2015.1030574

To link to this article: http://dx.doi.org/10.1080/15421406.2015.1030574

Published online: 06 Jul 2015.

Mol. Cryst. Liq. Cryst., Vol. 612: pp. 56–63, 2015

ISSN: 1542-1406 print/1563-5287 online
DOI: 10.1080/15421406.2015.1030574

Nematic Liquid Crystals under Conical Capillary Confinement: Theoretical Study of Geometry Effects on Disclination Lines

ALIREZA SHAMS,[1] XUXIA YAO,[2] JUNG OK PARK,[1,3] MOHAN SRINIVASARAO,[2,3,4] AND ALEJANDRO D. REY[1,*]

[1]Department of Chemical Engineering, McGill University, Montreal, Quebec, Canada
[2]School of Materials Science and Engineering, Georgia Institute of Technology, Atlanta, GA, USA
[3]Center for Advanced Research on Optical Microscopy, Georgia Institute of Technology, Atlanta, GA, USA
[4]School of Chemistry and Biochemistry, Georgia Institute of Technology, Atlanta, GA, USA

When a nematic liquid crystal is confined to a capillary tube with strong homeotropic anchoring conditions, unstable +1 disclinations lines can branch into a pair of +1/2 lines forming loops attached to the +1 axial line through branch points. The shape of the +1/2 disclination lines is a function of the confinement and the Frank elasticity. Our previous work shows that nematic liquid crystals under cylindrical confinement display a radial-to-planar polar defect texture transition through the nucleation and uniform motion of a disclination branch point that separates a high charge disclination from two lower charge ones. Here, we present the existence of a branch point for a nematic LC confined to different conical geometries with homeotropic anchoring. Determination of the defect geometry in conjunction with our model provides a means of characterizing the elasticity of LCs. Our results show that a larger conical angle reduces the length at which disclination curvature relaxes to zero and it also leads to less bending energy. These new findings are useful to assess the Frank elasticity of the nematic LCs and predict novel defect structures under confinement.

Keywords Nematic defects; branching disclination lines; conical confinement; disclination loops

1. Introduction

Nematic Liquid Crystals exhibit partial orientational order, symmetry-breaking phase transitions and characteristic defect textures [1–4]. Under non-planar confinement and strong anchoring conditions defect structures emerge and evolve based on frustration emanating from fixed orientation at curved bounding surfaces [5, 6]. Under cylindrical confinement, the stability of nematic textures depends on the capillary radius R and the temperature T (and concentration C as well for lyotropics). Stability conditions can be found in previous

*Address correspondence to Alejandro D. Rey, Department of Chemical Engineering, McGill University, Montreal, Quebec H3A 0C5, Canada. E-mail: alejandro.rey@mcgill.ca

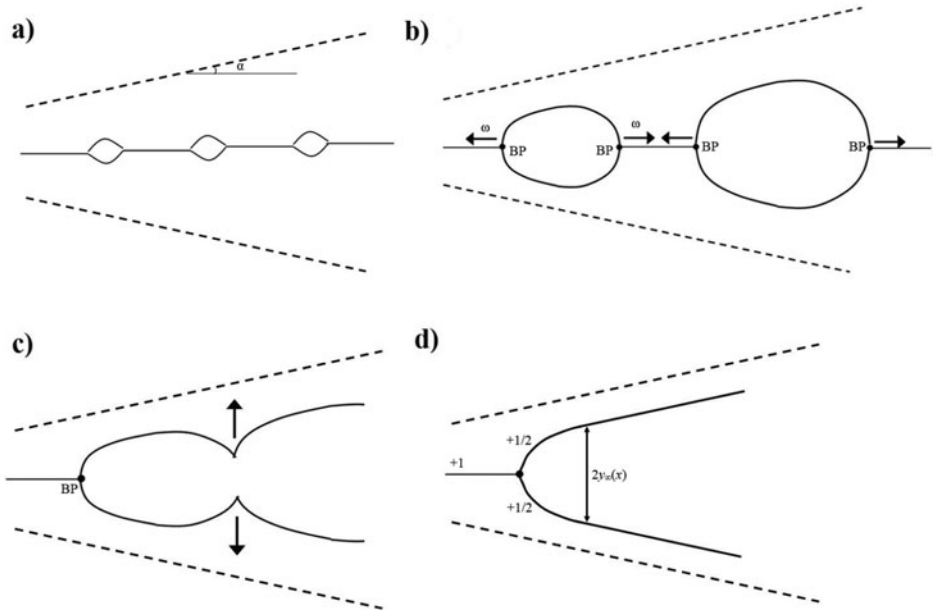

Figure 1. Schematics of the nucleation and growth process of domains consisting of +1/2 disclination loops that eventually lead to well-formed planar polar textures. **(a)** Initial nucleation stage, defect points appear on the axial +1 disclination line; **(b)** early growth stage including textural transitions from high order +1 disclination into energetically less costly $+\frac{1}{2}$ disclinations. The loops size depends on the local capillary size. The energy difference between the PP and PR textures (see text), generates the motion of the branch point (BP) but the branch point velocity varies along the cone angle; **(c)** Intermediate coarsening stage. The loop expansion stops when the loop vertical radius reaches the final defect distance, $y_\infty(x)$, but the BPs still move horizontally; **(d)** Final stage. After collision of the branch points, the relaxation of the line shape lead to 2 +1/2 disclination lines separated by distance $y_\infty(x)$.

studies [7, 8]. In our previous work [8, 9, 11], we focused on one possible transformation under capillary confinement, between the planar radial (PR) texture with a +1 axial singular disclination into a planar polar (PP) texture with a pair of off-axis +1/2 disclinations. Here, we consider the effect of conical confinement as opposed to cylindrical, on the texture transformation process. The nature of the PR→PP transition in principle can be explained by nucleation and growth (NG) [11] in which a number 'n' of +1/2 loops nucleate and grow along the initial +1 line. The distance L between nucleating loops is a function of capillary size; for a cylindrical confinement it can be estimated by $R_c = L/n$, where R_c is the capillary radius.

Figure 1 shows a schematic of the NG mode of the PR→ PP transition in a conical capillary which includes the following stages: (a) initial stage: nucleation on a pre-existing +1 line with "n" +1/2 loops; (b) early stage: growth of +1/2 loops, involving the axial motion of branch points (BP) that joins the +1/2 loops and the +1 line segments with a constant branch angle. Because the capillary radius is a function of axial location, the sizes of loops are different and also the branch points move with different velocities; (c) intermediate stage: coarsening and vertical growth saturation of the +1/2 loops, where the vertical saturation is $2y_\infty(x) = 1.33R$; here R is the local capillary radius which is a function

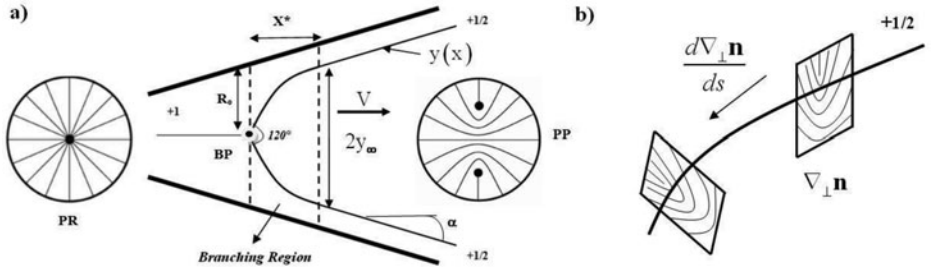

Figure 2. (a) Schematic of the anchoring-driven textural transformation in a cylindrical capillary of diameterr D = 2R, from the planar radial (PR) texture with a +1 singular disclination line along the capillary, into a planar polar (PP) texture with a pair of +1/2 disclinations. The branch point BP moves leftwards with a constant velocity V since the elastic energy of the PR texture is larger than the PP one. The motion is shape invariant. The disclination branching process is characterized by the shape of the emanating +1/2 lines and their aperture angle. The branch point is denoted by the black dot. **(b)** Orientation gradients on the plane perpendicular to the line contain splay-bend distortion and generate line tension. The additional orientation gradient distortions along the arc length generate bending. [Adapted from ref.10].

of the cone angle, α, the initial radius, R_0, and the axial distance "x":

$$\mathrm{R} = \mathrm{R}_0 + \mathrm{x}\tan(\alpha) \tag{1}$$

and (d) late stage: formation of the PP texture with two parallel +1/2 lines separated by a distance $2y_\infty(x)$. The early stage and loop growth have been investigated for confined nematics in cylindrical geometries [11, 12]; here we focus on the early and late stages, characterization of the branching process and the effect of the conical confinement. The intermediate stage will be investigated in future work.

The specific objectives of this paper are: to model the disclination branching arising in typical texture transitions and predict the shape of disclination loops under conical capillary confinement under strong homeotropic anchoring.

The organization of this paper is as follows. Section 2 presents the theoretical framework and equations that govern disclination branching and the loop growth process. Section 3 presents the computational results, including disclination loop growth, disclination curvature and space curve as a function of arc-length and length of confinement, the effect of cone angle and initial radius on the disclination shape and energy, and the relations between geometric parameters and disclination elasticity. Section 4 presents the conclusions. This paper builds on our previous work on nematic liquid crystals under cylindrical confinement [8–10]. As mentioned above the analysis is restricted to statics with the assumption that under the motion of BPs, the curve $y(x)$ shape is dictated by elasticity and not by viscous dissipation.

2. Theory

2.1. Disclination Curve

Figure 2(a) shows a schematic of textural transformation studied in this paper for a conical confinement, using the standard Frank-Oseen liquid crystal director **n** model [1], here

depicted by the thin lines inside the two circles (PR, PP). The three disclination lines (one +1 and two +1/2) meet at the branch point (BP). As the energy of the PR texture is higher than the PP, the BP region moves slowly to the left [10]. Figure 2(b) shows the orientation distortions associated with a curved +1/2 disclination line. Orientation gradients on the plane perpendicular to the line ($\nabla_\perp \mathbf{n}$) contain splay-bend distortion and generate line tension. The additional orientation gradient distortions along the arc length ($d\nabla_\perp \mathbf{n}/ds$)generate bending elasticity.

The Frank gradient elasticity density f for uniaxial Nematic LCs, using the one constant approximation is [1]:

$$f = \frac{K}{2}\left((\nabla \cdot \mathbf{n})^2 + (\nabla \times \mathbf{n})^2\right) \tag{2}$$

where $\mathbf{n}$ is the director field whose minimum satisfies the Euler Lagrange equation $K\nabla^2\mathbf{n} = \lambda\mathbf{n}$, K is the Frank elastic constant, and λ is a Lagrange multiplier that takes into account the restriction $\mathbf{n}.\mathbf{n} = 1$. Using a planar director parameterization $\mathbf{n} = (\cos\psi, \sin\psi, 0)$ and planar polar coordinates (r,ϕ), a wedge disclination solution, located at the coordinate origin, to the Euler Lagrange equation is $\psi = \mathrm{m}\phi + \mathrm{C}$, where m is a multiple of $\pm 1/2$ and C is a constant. The energy per unit length of a straight disclination line $\gamma(\kappa = 0) = \gamma_0$ obtained by integrating the free energy density f (Equation (1)) is:

$$\gamma_o = \frac{1}{L}\int_{r_c}^{R}\int_{0}^{2\pi}\int_{0}^{L} \mathrm{frdrd}\varphi ds + \pi\sigma_c \mathrm{r_c^2} \tag{3}$$

where $\mathrm{r_c}$ is the core radius and σ_c the core energy density, which can be estimated to be $\sigma_c \approx \mathrm{m^2 K r_c^2}$ and is typically assumed to be ignorable compared to other terms. Integrating the Frank elastic energy in a local polar coordinate system yields the line tension γ as a sum of straight γ_0, and bending $\mathrm{k_c}\,\kappa^2/2$ contributions [10]:

$$\gamma = \gamma_o + \frac{\mathrm{k}_c}{2}\kappa^2,\ \gamma_o = \frac{\mathrm{K}\pi}{4}\ln\left(\frac{\mathrm{R}_0 + x\tan(\alpha)}{r_c}\right),\ k_c = \frac{K\left(\mathrm{R}_0 + x\tan(\alpha)\right)^2\pi}{\sqrt{2}} \tag{4a, b, c}$$

where $\mathrm{k_c}$ is the bending modulus. Equations (4) indicates that the bending effect becomes significant at $\kappa \approx 10^{-2}\mu\mathrm{m}^{-1}$. This demonstrates the role of bending on disclination line shape.

To describe the disinclination shape we need to formulate the line stress tensor and then substitute this tensor into the line force balance equation. Assuming that the entire disclination branching region is moved because the energy of the PR region is higher than the energy of the PP region (see refs. [8, 9] for full details), the shape changes occur much faster than the convection. By considering the stress balance [13], we find the disclination shape equation in the local approximation:

$$\gamma_{0,1/2}\kappa - k_c\left(\kappa_{ss} + \frac{\kappa^3}{2}\right) = 0 \tag{5}$$

Due to the disclination bending, the "diffusive" term $\mathrm{k_c}\kappa_{ss} = \mathrm{k_c}\partial^2\kappa/\partial s^2$ and the nonlinearity $\mathrm{k_c}\kappa^3/2$ arise. For the loop growth and pre-saturated stages the line viscosity term is negligible comparing to other terms [11] but it becomes important in the relaxation mode. The two important parameters in Equation 5 are the disclination curvature at the branch

point, $\kappa_0 = \mathrm{d}\phi/\mathrm{ds}|_{s=0}$, and the stiffness ratio "a" (1/ length^2) of tension to bending moduli:

$$a(\alpha, R_0,) = \frac{\gamma_{\mathrm{o},1/2}}{\mathrm{k_c}} = \frac{\ln\left(\frac{(R_0 + x\tan\alpha)^2}{2\mathrm{y}_x \mathrm{r_c}}\right)}{\sqrt{1.68\,(R_0 + x\tan\alpha)}} \tag{6}$$

where "x" and "y" are found by integrating $\mathrm{d}x/\mathrm{ds} = \cos\theta$ and $\mathrm{d}y/\mathrm{ds} = \sin\theta$[14]:

$$x\,(s, a, \kappa_o) = \int_0^s \cos(\theta)\mathrm{ds}'; \mathrm{y\,(s,\,a,}\,\kappa_0) = \int_0^s \sin(\theta)\mathrm{ds}' \tag{7}$$

where the normal angle θ is found from by integration of the curvature $\kappa = d\theta(s)/ds$[10]:

$$\theta(s) = \alpha + \frac{\pi}{2} + \int_s^\infty \kappa(s', a, \kappa_0)ds' \tag{8}$$

To satisfy the boundary conditions, normal angle is $(\theta(s = 0) = 5\pi/6)$at the BP and $(\theta(s \to \infty) = \alpha + \pi/2)$ at the far field. The defect separation distance y_∞ far from BP is found from

$$y\,(\kappa \approx 0) = y_\infty(x) = 0.665R(x) \tag{9}$$

The branch point is located at (x = 0, y = 0). The branch point angle φ is given by$\lim_{x\to 0} \partial y/\partial x \to \tan\varphi$. The branch point angle is a function of elastic properties and can be found from experiments and theory by fitting the shape (x,y). In the following section we derive an equation to find the branch point angle.

2.2. Single Loop Growth

Equation 5 also can be used to model the loop growth shown in Fig.1b. The boundary conditions for the loop growth stage written in terms of y and x are:

$$\begin{cases} x = 0, \mathrm{y} = y_0(t) \\ x = X_B(t), \mathrm{y} = 0, \left.{}^{dy}/_{dx}\right|_{x_b} = \tan(\varphi) \end{cases} \tag{10}$$

It should be emphasized that the branch point velocity and the frustum length, $\mathrm{X_B}$, vary based on the loop location in the cone. In partial summary, the integrated model calculates the disclination curvature $\kappa(s)$ and curve $y(x)$ that describe the branching process in a conical frustum.

3. Results and Discussion

3.1. Early Stage

Figures 3(a) shows the rate of change in branch point curvature as a function of time. For the branch point on the left side we have a competition between two effects. When the branch point moves to the left side, the decreasing capillary radius promotes more curvature [8, 9] but this movement also increases the loop size and promotes less curvature [10]. These two opposite effects result in a smooth change for the left branch point curvature which decreases over time. On the other hand, the rate of changes is higher for the right branch

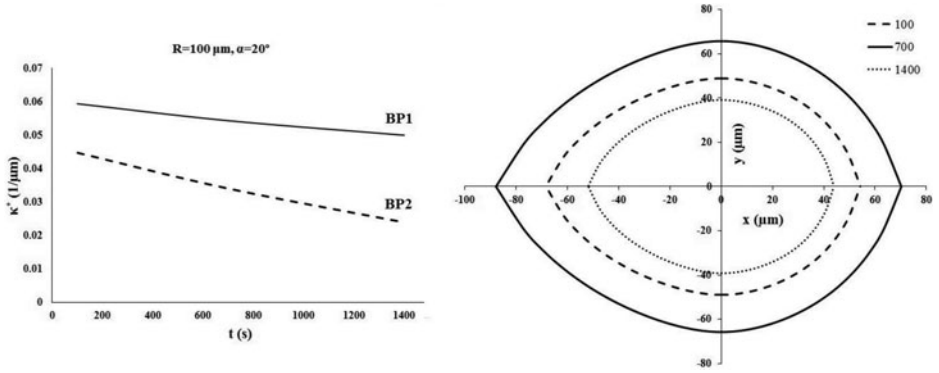

Figure 3. **(a)** The branch points curvature as a function of time for $\alpha = 20^\circ$ and $R_0 = 100\ \mu$m; **(b)** The disclination curves for a cone angle $\alpha = 20^\circ$ for $t = 100$, 700 and 1400 s. The loop size increases over time.

point because these two effects act in a cooperation to decrease the curvature. Figure 3(b) shows representative disclination curves $y(x)$ for a cone angle $\alpha = 20^\circ$ for $t = 100$, 700 and 1400 s. It can be seen that at the beginning, loops are symmetrical but because the left branch point moves faster than the right one, the shape becomes more and more asymmetric. For smaller cone angles, loops are more symmetrical compared to larger cone angles. At the final stage, X_{B1} is around 80 to 100 μm and X_{B2} is around 70 to 80 μm for cone angles between 10° to 20°. For smaller cone angles, the difference between the branch point velocities for both sides are small, so X_{B2} is close to X_{B1}, but by increasing the cone angle, X_{B1} becomes much larger than X_{B2} and the loops turn out to be egg-shaped.

3.2. Late Stage

Figure 4(a) shows the tension to bending stiffness ratio (k_c/γ_0) as a function of R_0 for different values of the cone angle at arc-length = 200 μm. It can be seen that for weak

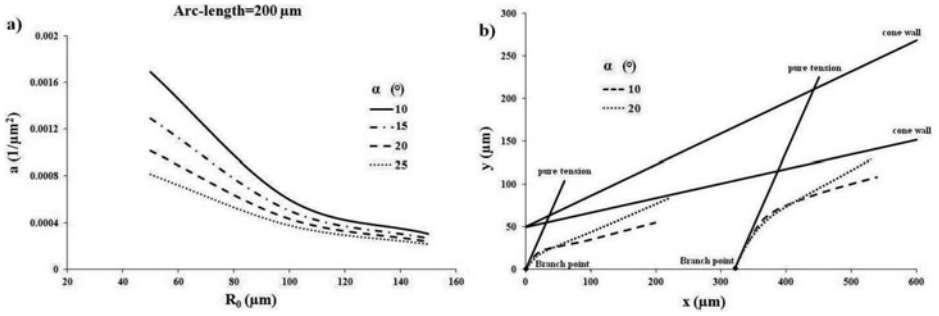

Figure 4. **(a)** The tension to bending stiffness "a" as a function R_0 for $\alpha = 10^\circ$, 15°, 20° and 25° at arc-length = 200 μm. This ratio decreases in scale of R^2 and the rate of changes is faster for smaller radius. For R_0>100 μm, the effect of cone angle becomes ignorable; **(b)** The effect of branch point movement along the cone axis for different cone angles. The effect of increasing the initial radius and the cone angle is the same and result in increasing the bending energy and tilting the disclination curve to a pure tension line.

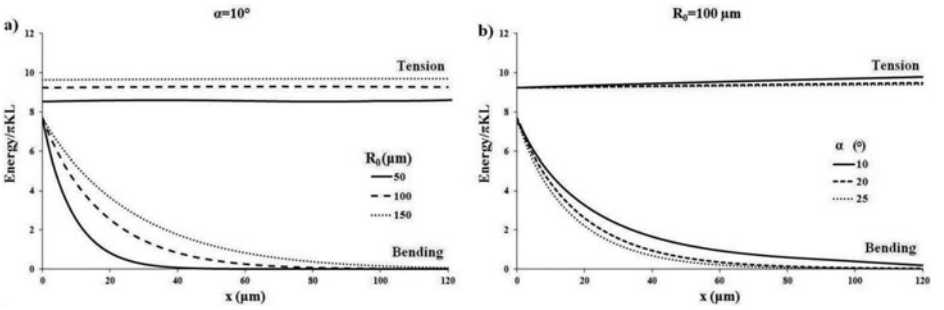

Figure 5. **(a)** The tension and the bending energies as a function of distance for α: 10° and $R_0 = 50$, 100 and 150 μm. The bending energy is affected more than the tension energy by the cone radius; **(b)** The tension and the bending energies as a function of distance for $R_0 = 100$ μm and $\alpha = 10°$, 20° and 25°.

confinement (large R_0), this ratio becomes almost independent of the cone angle which means the only effective parameter on the geometry and the energy of the disclination line is the cone radius. The geometry effects are summarized in Fig. 3(b) which shows the disclination curves for two different cones with angles of 10° and 20°. In a cone, motion of the branch point along the cone angle increases the initial radius resulting in tilting the curve to the pure tension line and reducing the bending moduli. The same movement of branch point in a cone with a lager cone angle shows more changes because a larger tan(α) with the same R_0 and the same x results in a larger R.

To characterize the different energies we introduce: (*i*) the total tension energy E_t, and (*ii*) the total bending energy E_b:

$$E_T = \int_0^{S^*} \gamma_{o,1/2} ds = \int_0^{X*} \gamma_{o,1/2} \operatorname{cosec}\theta\,(x)\,dx; E_b = \int_0^{S^*} \left(\frac{k_c}{2}\kappa\,(s)^2\right) ds \qquad (11)$$

where S^* is the arc-length at which the curvature is nearly zero and X^* is the frustum height at which the disclination curve y(s) achieves linearity. According to Equation 4(c), the rate of changes for bending can be scaled by $1/(R_0+x\tan(\alpha))^2$, the tension energy is not a strong function of the initial radius or cone angle. Figure 5(a) shows the tension and the bending energies along the cone angle for $\alpha = 10°$ and $R_0 = 50$, 100 and 150 μm. By increasing the radius, the bending energy increases more than the tension energy, and the ratio of tension to bending decreases. Figure 5(b) shows the tension and the bending energies as a function of x for $R_0 = 100$ μm and $\alpha = 10°$, 20° and 25°. The same thing happens here and by increasing the cone angle, the ratio of tension energy to bending energy decreases, but the effect of the cone angle is weaker than the effect of the cone radius.

Conclusions

Nematic liquid crystals under conical capillary confinement are predicted to display a behavior similar to the cylindrical confinement case, including a variety of textures according to the initial capillary radius R_0, the cone angle α and the temperature (and the concentration as well for lyotropes). In the present paper, we showed that under conical confinement the branching of a +1 into a pair of +1/2 curved disclinations is modified by gradients in confinement as well as the cone aperture α. Because the cone radius changes

along the cone axis, the disclination loops are egg-shaped and at any given time they are of different sizes. Gradient in confinement ($dR/dx = \tan\alpha$) increases the bending stiffness while larger aperture (α) decreases total curvature, creating a competition that results in lower total curvatures but greater total elasticity. The specific predictions made in this paper can be used to nematic texture transitions in linear and hyperbolic cones, in biological microfluidics, and mesophase fiber spinning.

Funding

This work is supported by a grant from the U.S. Office of Basic Energy Sciences, Department of Energy; grant DE-SC0001412.

References

[1] de Gennes, P. G. (1995), *The Physics of Liquid Crystals*, Oxford University Press: New York, USA.
[2] Kleman, M. & Lavrentovich, O.D. (2003). *Soft Matter Physics*, Springer-Verlag: New York, USA.
[3] Virga, E. G., (1994) *Variational Theories for Liquid Crystals*, Chapman Hall: London, UK.
[4] Stewart, I. W. (2004) *The Static and Dynamic Continuum Theory of Liquid Crystals: A Mathematical Introduction*, Taylor & Francis: New York, USA.
[5] Crawford G. P., & Zumer, S. (1996) *Liquid Crystals in Complex Geometries: Formed by Polymer and Porous Networks*, Taylor & Francis: London, UK.
[6] Rey, A. D. (2010). *Soft Matter*, *6*(5), 3402; Rey, A.D. (2007). *Soft Matter*, **2**, 1349; Rey, A.D., & Herrera Valencia, E. E. (2014). *Soft Matter*, **10**, 1611; Wincure, B., & Rey, A.D. (2007) *Liquid Crystals*, **34(12)**, 1397; Gupta, G. & Rey A. D., (2005) *Phys. Rev. Lett.* **95(12)**, 127805.
[7] Yan, J., & Rey, A. D. (2002). *Carbon*, 2002, *40*, 2647; (2002). *Phys. Rev. E*, **65**, 031713; (2003). *Carbon*, **41**, 105.
[8] Shams, A., Yao, X., Park, J. O., Srinivasarao, M. & Rey, A. D. (2012). *Soft Matter*, *8*, 11135.
[9] Shams, A., Yao, X., Park, J. O., Srinivasarao, M. & Rey, A. D. (2013). *Mater. Res. Soc. Symp. Proc.*, 1526; Yao, X., Rey, A. D., Park, J. O., & M. Srinivasarao, M. (2012). Lyotropic chromonic liquid crystals in the biphasic region, *APS March Meeting Processing*, 57(1).
[10] Shams, A., Yao, X., Park, J. O., Srinivasarao, M. & Rey, A. D. (2014). *Soft Matter*, *10*, 3245.
[11] Shams, A., Yao, X., Park, J. O., Srinivasarao, M. & Rey, A. D. (2014). *Phys. Rev. E*, *90*(4), 042501.
[12] De Luca, G. & Rey, A. D. (2007) *J. Chem. Phys.*, *126*, 094907; (2007) *J. Phys. Chem.*, **127**, 104902/1.
[13] Gurtin, M. E. (1993) *Thermomechanics of Evolving Phase Boundaries in the Plane*, Oxford University Press: New York, USA.
[14] Ludu A. (2007). *Nonlinear Waves and Solitons on Contours and Closed Surfaces*, Springer-Verlag: Berlin, Germany.